# 論文内容の要旨

## 論文題目　Cation Ordering and Electrical Properties of Double Perovskite Molybdate Thin Films

## （二重ペロブスカイト型 Mo 酸化物薄膜における カチオン配列と電気物性の研究）

氏名　重松　圭

**I. Introduction**

Transition-metal oxides with the double-perovskite structure $A_2BB'O_6$ are known to exhibit a variety of electronic properties, such as room temperature magnetoresistance in $Sr_2FeMoO_6$ and magnetodielectric properties in $La_2NiMnO_6$, depending on the combination of *B*- and *B'*-site cations. Among them, $Sr_2MgMoO_6$ (SMM), of which the crystal structure is shown in Figure 1, has attracted much attention as a promising anode material for hydrocarbon-fueled solid-oxide fuel cells (SOFCs), because of its high tolerance to carbon deposition and sulfur poisoning, which enables the direct use of natural gas fuel instead of hydrogen in SOFCs [1].

An important influence on the performance of anode materials in fuel cells is electrical conductivity. Although stoichiometric SMM with $d^0$ $Mo^{6+}$ is a typical insulator, SMM tends to contain oxygen vacancies ($Sr_2MgMoO_{6-\delta}$) at high temperatures under reductive atmospheres, which are the typical working conditions for SOFC anodes. Because of this, the oxygen-vacant SMM conducts current because of the mixed valence state of $Mo^{5+}$ and $Mo^{6+}$. However, SMM's conductivity, $\rho$, has been reported to fall between $10^{-1}$ and $10^{1}$ Ω cm even at 800°C, which does not meet the practical requirement of $\rho < 10^{-2}$ Ω cm under typical operating conditions. One central reason for the poor $\rho$ is that the amount of oxygen vacancies in SMM is limited to $\delta$ = 0.046 so long as SMM is synthesized by a conventional solid-state reaction at equilibrium, although $\delta$

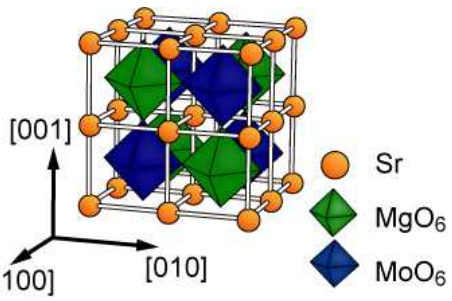


Fig. 1. Schematic illustration of perfectly ordered double perovskite structure of $Sr_2MgMoO_6$.

increased as *B*-site ordering ratio decreased [2]. In bulk SMM, Mo ions favor the hexavalent state and tend to be ordered alternately with $Mg^{2+}$, due to the large difference in their ionic charges. Thus, the use of a non-equilibrium synthetic approach might further increase Mg/Mo disorder and enhance $\delta$, beyond the limitation imposed by conventional solid-phase reactions.

In this study, I have fabricated oxygen-vacant SMM thin films by pulsed laser deposition (PLD), which enables the growth of thin films in non-equilibrium conditions because of the large kinetic energies of ablated plumes. I also investigated the crystal structure, electronic states, and electrical conductivity of the SMM thin films.

**II. Experimental**

A polycrystalline SMM pellet, used as the PLD target, was synthesized from mixed powders of $SrCO_3$, MgO, and $MoO_3$ by a solid-state reaction. SMM thin films were deposited on $SrTiO_3$(111) (STO) substrates under four different conditions, where the substrate temperature ($T_s$) and oxygen partial pressure ($P_{O2}$) were varied as the main growth parameters: Sample I was fabricated at ($T_s$, $P_{O2}$) = (800°C, $10^{-4}$ Torr); Sample II at (700°C, $10^{-4}$ Torr); Sample III at $T_s$ = 700°C under a base pressure of ~$1\times10^{-8}$ Torr; and Sample IV at $T_s$ = 800°C under the same base pressure. The fourth harmonic of a Nd:YAG laser (wavelength = 266 nm) with energy density of 0.3 J/cm$^2$/shot and a repetition rate of 2 Hz was employed to ablate the target. The typical thickness of the films was ~50 nm. Crystal structures were characterized with x-ray diffraction (XRD). Mo 3*d* core-level and valence-band spectra were measured by hard x-ray photoemission spectroscopy (HAXPES) using BL47XU at the SPring-8 facility. The spectra were collected by a Scienta R-4000 electron energy analyzer, with energy resolution of 0.3 eV at the photon energy of 7.94 keV. DC resistivity was measured by the four-probe method. The carrier type was confirmed with Hall effect measurements.

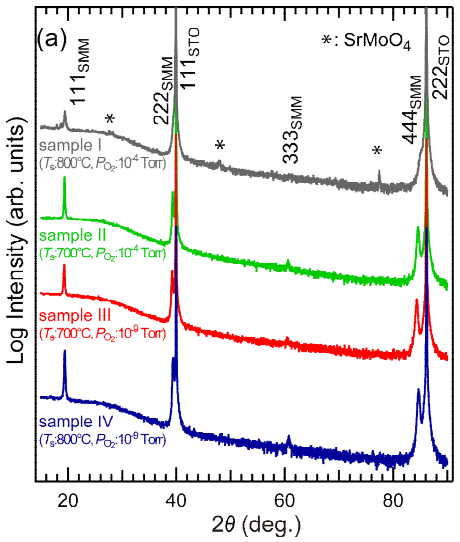


Fig. 2. Out-of-plane $2\theta$-$\theta$ XRD patterns of SMM thin films on STO(111) substrates. Asterisks indicate secondary-phase $SrMoO_4$ diffraction peaks.

**III. Results and Discussion**

Figure 2 shows out-of-plane $2\theta$-$\theta$ XRD patterns of the fabricated SMM thin films. Here I used an assumption that a unit cell of SMM can be regarded as a pseudo-cubic double perovskite. All the samples exhibited *hhh* diffraction peaks from the SMM film and STO substrate, indicating epitaxial growth of (111)-oriented SMM films on the STO substrates. In Samples II–IV, no secondary phase, such as Mo, MgO or $SrMoO_4$, was detected, whereas Sample I showed diffraction from a secondary phase of $SrMoO_4$. The out-of-plane spacing $d_{111}$ of Sample I was calculated to be 4.556 Å, which is almost the same as 4.554 Å of bulk SMM ($\delta \sim 0$), while the $d_{111}$ values of Samples II–IV were considerably larger than that of Sample I, as can be seen from the shifts in the SMM peaks to the lower $2\theta$ side. This suggests that considerable oxygen vacancies were introduced to Samples II–IV. Notably, the full width at half maximum (FWHM) values of the SMM 222 rocking curves were almost constant, 0.6º, proving that Samples II–IV have equivalent crystallinity.

Figure 3 shows a typical two-dimensional $2\theta$-$\chi$ image around the STO 110 and SMM 220 diffraction peaks. The SMM

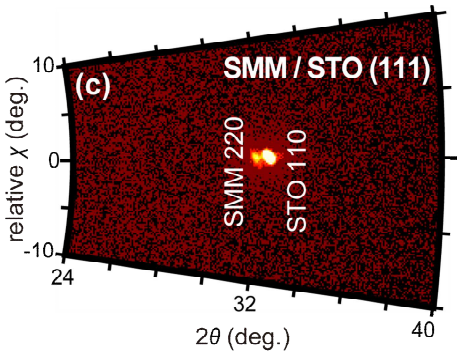


Fig. 3. Typical XRD image of a two-dimensional $2\theta$-$\chi$ scan around the in-plain diffraction of STO 110 and SMM 220.

220 diffraction peak was located at the same $\chi$ position as the STO 110 peak at $\chi$ = 54.7º, indicating that the SMM films were free from lattice strain from the STO substrate, which is likely due to the large lattice mismatch at the interface.

I use the intensity ratio of the 111 superstructure peak to the 222 fundamental peak, $r_{111/222}$ as a measure of the degree of *B*-site ordering. The resulting $r_{111/222}$ values for Samples II, III, and IV were 1.33, 1.21, and 1.13, respectively; suggesting that $\delta$ decreases most in Sample IV, less in Sample III, and the least in Sample II. It was difficult to evaluate $r_{111/222}$ in Sample I due to the severe overlap of the SMM 222 diffraction peak with the STO 111 peak. In perfectly ordered SMM, the $r_{111/222}$ ratio should be 2.83 for a 50 nm-thick film. Using this value, the Mg/Mo ordering ratio is estimated to be 69%, 65% and 63% for Samples II, III, and IV, respectively.

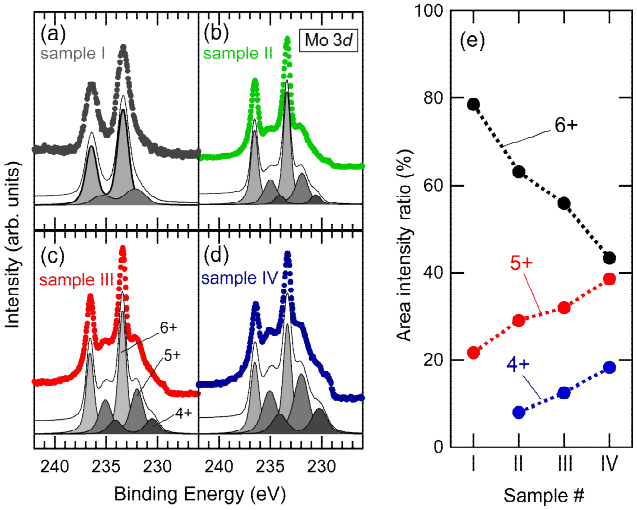


Fig. 4. Mo 3*d* core-level HAXPES spectra of (a) Samples I, (b) II, (c) III, and (d) IV. Solid curves represent the components of 6+ (square), 5+ (triangle), and 4+ (circle) states obtained by least-square fitting. In the spectrum of Sample I, the peak position of $Mo^{6+}$ $3d_{5/2}$ was fixed to 233.4 eV to calibrate the charge-up shift. (e) Plot of area ratios of the $Mo^{6+}$, $Mo^{5+}$, and $Mo^{4+}$.

In order to probe the intrinsic electronic states of SMM thin films that are free from surface effects, I adopted HAXPES, which allows us to perform bulk-sensitive spectroscopy with a probing depth of ~10 nm. Figures 4(a)–(d) depict the Mo 3*d* core-level HAXPES spectra for Samples I–IV, respectively. The Mo 3*d* spectra were reproduced well by combining the $3d_{5/2}(3d_{3/2})$ components of $Mo^{6+}$, $Mo^{5+}$, and $Mo^{4+}$, corresponding to the peaks located at the binding energies ($E_b$) 233.3(236.5), 232.0(235.0), and 230.4(234.1) eV, respectively. The fractions of individual Mo components, $f(Mo^{6+})$, $f(Mo^{5+})$ and $f(Mo^{4+})$, calculated from the peak area intensities are presented for comparison in Fig. 4(e). The $Mo^{6+}$-component fraction tended to decrease in succession from Samples I to IV, whereas those of $Mo^{5+}$ and $Mo^{4+}$ increased. This suggests that $\delta$ increases in this order, which is consistent with the above argument regarding $r_{111/222}$. Assuming that $Mo^{6+}$ is reduced to $Mo^{5+}$ and $Mo^{4+}$ by the formation of oxygen vacancies, $\delta$ can be deduced by using the relation $\delta = f(Mo^{5+})/2 + f(Mo^{4+})$. The calculated $\delta$ values are 0.22, 0.28, and 0.37 for Samples II, III, and IV, which are indeed much larger than the maximum $\delta$ in bulk, 0.046.

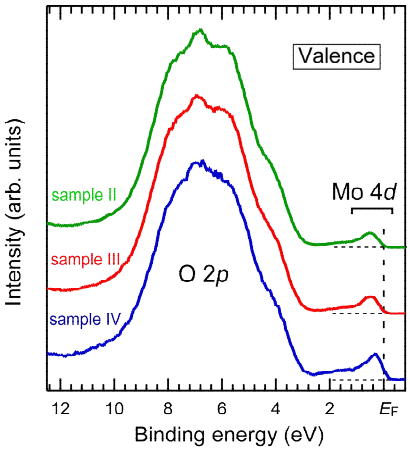


Fig. 5. HAXPES valence-band spectra of Samples II–IV near the Fermi level.

Figure 5 shows valence-band HAXPES spectra for Samples II–IV. All of the samples exhibited two peaks: a prominent peak located at $E_b$ = 3–10 eV, derived from O 2*p*, and another smaller peak near the Fermi energy ($E_F$). Similar structures were observed in the valence-band PES spectrum of oxygen-vacant $MoO_{3-\delta}$. According to density function theoretical calculations for stoichiometric SMM ($\delta$ = 0), the bottom of the conduction band is dominated by the 4*d*-orbital of $Mo^{6+}$ ($d^0$). Comparing Fig. 5 with the experimentally observed valence-band spectra of $MoO_{3-\delta}$ and the theoretically predicted band structure of SMM, the peak near $E_F$ can be attributed to a Mo 4*d* band composed of $Mo^{5+}$ ($d^1$) and $Mo^{4+}$ ($d^2$) states.

Finally, I discuss the electrical resistivity ($\rho$) of the SMM films as a function of temperature (*T*), as shown in Fig. 6. The $\rho$(300 K) values of Samples II–IV were 6.6 × $10^{-2}$, 5.7 × $10^{-2}$, and 2.7 × $10^{-2}$ Ω cm,

respectively, and tended to decrease with increasing $\delta$ in the samples. Notably, these resistivity values were substantially lower than those reported for polycrystalline samples synthesized by solid-state reactions, which are > $10^1$ Ω cm at 800°C. However, Sample I performs as an insulator with $\rho$ > 10 Ω cm at 300 K. The Hall coefficients of the SMM films were negative, supporting the conclusion that electrons generated by oxygen vacancies served as carriers. Considering the XRD and HAXPES results, I concluded that the difference in conductivity among Samples II–IV is due to the variation of the amount of oxygen vacancies.

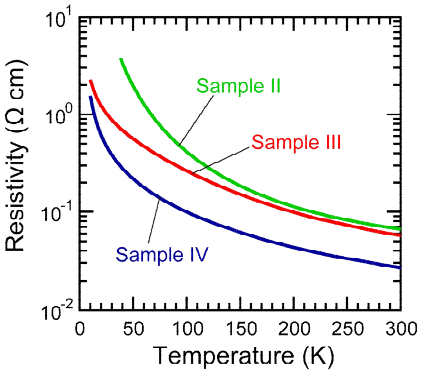

Fig. 6. Resistivity of Samples II–IV as a function of temperature.

**IV. Conclusion**

I successfully fabricated epitaxial thin films of SMM containing a sizable amount of oxygen vacancies, depending on the substrate temperature and oxygen partial pressure during PLD growth. The XRD intensity ratio $r_{111/222}$, which is a measure of the Mg/Mo ordering, was much smaller than those for bulk samples, indicating that extensive *B*-site disorder was introduced into the SMM films. The SMM films showed remarkably low resistivity values, within the range of 2.7−6.6 × $10^2$ Ω cm at 300 K, and these varied systematically with respect to the $r_{111/222}$ and $\delta$ values estimated from the HAXPES result. This study indicates the possibility of improving properties of *B*-site ordered double perovskites by introducing disorder in *B*-sites.

**References**

[1] Y.-H. Huang *et al.*, Science **312**, 254 (2006).
[2] C. Bernuy-Lopez *et al.*, Chem. Mater. **19**, 1035 (2007).